1-23-2012

An extremely low profile, compact, and broadband tightly coupled patch array

E. Irci
The Ohio State University

K. Sertel
The Ohio State University

John L. Volakis
The Ohio State University

An extremely low profile, compact, and broadband tightly coupled patch array

E. Irci,[1] K. Sertel,[1] and John L. Volakis[1]

Received 10 May 2011; revised 15 August 2011; accepted 31 October 2011; published 17 January 2012.

[1] A tightly coupled patch array (TCPA) is introduced to realize small-size, extremely low profile planar antennas with broadband performance. Past approaches have used frequency selective surfaces (FSSs) as part of the substrate or ground plane (i.e., in passive mode) for also realizing low-profile antennas. In contrast, the proposed TCPA employs an FSS aperture as the radiating structure (i.e., array antenna). A key aspect of the TCPA is the exploitation of differences in FSSs when operating in radiating and passive modes. Tight element coupling and periodic excitation are the keys for achieving broadband operation. In this paper, a small-size, finite array is designed along with a very thin and compact feeding network. The designed TCPA resonated at 2.07 GHz with 5.6% impedance bandwidth ($|S_{11}| < -10$ dB), 4.4 dB realized gain (86% efficiency), and 23% gain bandwidth (3 dB drop). Of importance is that the overall aperture dimensions were only $\lambda_0/3 \times \lambda_0/3$ and $\lambda_0/42$ thick (including feeding network) at the midfrequency of operation. A preliminary TCPA antenna prototype was fabricated and tested. Both simulated and measured data show enhanced bandwidth as compared to the conventional microstrip patch antennas of the same size and thickness. However, as common for such extremely low profile microstrip antennas, the conductivity losses were augmented. Thus, the measured TCPA efficiency (50%) was smaller than computed.

Citation: Irci, E., K. Sertel, and J. L. Volakis (2012), An extremely low profile, compact, and broadband tightly coupled patch array, *Radio Sci.*, *47*, RS0M06, doi:10.1029/2011RS004771.

1. Introduction

[2] Miniaturization of microstrip antennas, especially reducing their profile, without sacrificing operational bandwidth, gain and radiation properties continues to be a major challenge. Recently, artificial periodic structures brought significant remedies in overcoming this issue. A successful realization was the periodic mushroom-type electromagnetic band gap (EBG) structure, which formed a high-impedance surface (HIS) [*Sievenpiper et al.*, 1999]. Such surfaces suppress surface waves and mimic perfect magnetic conductors (PMCs). Hence, they form an artificial magnetic conductor (AMC) ground plane [*Sievenpiper et al.*, 1999; *Goussetis et al.*, 2006]. In contrast to conventional metallic ground planes that generate an out-of-phase (180°) reflection, the AMCs have an in-phase (0°) reflection albeit with limited bandwidth. Thus, the AMC reflected wave adds constructively with direct aperture radiation. This allowed for realizing low-profile antennas [*Sievenpiper et al.*, 1999; *Goussetis et al.*, 2006; *Feresidis et al.*, 2005], with broadband performance [*Bell and Iskander*, 2004; *Bell et al.*, 2007; *Erdemli et al.*, 2002]. Suppression of surface waves also lead to reduced mutual coupling between microstrip antennas [*Yang and Rahmat-Samii*, 2003a].

[3] Instead of utilizing mushroom-type structures as AMCs, in the work by *Yang and Rahmat-Samii* [2003b] return losses of low-profile wire antennas were enhanced by tailoring the EBG's reflection phase. For this case, reflection phase was in the 90° ± 45° range and led to improved impedance bandwidth when the EBG acted like neither perfect electric conductor (PEC) nor PMC, but in their middle. Alternatively, metallic patches placed on metal-backed high-contrast dielectrics were employed by *Mosallaei and Sarabandi* [2004] to create reactive impedance substrates (RISs) that could be tuned to operate anywhere between PEC and PMC ground planes. Similar to *Yang and Rahmat-Samii* [2003b], the impedance bandwidth and radiation performance of low-profile wire and patch antennas were improved when the RIS was neither PEC nor PMC, but at an optimal reactive value in between.

[4] Essentially, the periodic structures in previous efforts are frequency selective surfaces (FSSs) [*Munk*, 2000; *Vardaxoglou*, 1997] in passive mode, which are employed as substrates or ground planes to other radiating elements. The latter can be any element of choice; including dipole, patch, spiral and their array version. However, in this setup, the overall antenna bandwidth is limited by the excited element or the passive FSS, depending on which one is smaller. Also, the excited element usually may not illuminate the FSS in a manner (i.e., as a uniform plane wave) to realize the ideal FSS reflection coefficient. Further, the FSS substrate implies significant thickness (in most cases 2/3 of overall thickness), which hinders reducing the antenna profile.

[1]ElectroScience Laboratory, Department of Electrical and Computer Engineering, Ohio State University, Columbus, Ohio, USA.

0048-6604/12/2011RS004771

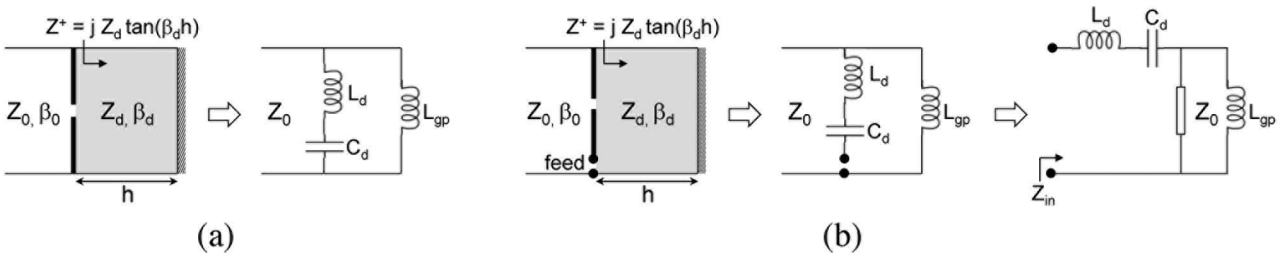

Figure 1. Circuit model representations of FSSs. (a) Passive mode. (b) Radiating mode.

[5] In this work, we present an alternative methodology to realize very low profile and small-size microstrip antennas. The resulting design enjoys broad bandwidth, high gain and good radiation performance. This is accomplished by using the FSS itself as the radiating aperture (i.e., operating the FSS as array antenna). This approach was first envisioned by Benedikt A. Munk when he proposed the current sheet array (CSA) [*Munk*, 2003; *Munk et al.*, 2003]. The tightly coupled patch array (TCPA) proposed here was therefore inspired from the CSA functionality. However, there are several differences between the CSA and TCPA. Among them are the following:

[6] 1. The CSA is an ultra wide band (UWB) antenna demonstrated to reach 4.5:1 impedance bandwidth (for VSWR < 2) without any dielectric substrates/superstrates, even though it is $\lambda_0/10$ thick at the lowest operational frequency. On the contrary, the TCPA employs a high-contrast dielectric substrate for miniaturization and achieves $\lambda_0/50$ profile. Thus, its bandwidth is much narrower as a consequence of the thinner profile.

[7] 2. In CSA design, dielectric materials are suggested as superstrates rather than substrates, to improve the bandwidth up to 9:1 and to obtain better scan capability [*Munk*, 2003]. In TCPA, the opposite is done for achieving a very low profile. In addition, only broadside radiation is considered. Scanning capabilities are discarded, although would be feasible.

[8] 3. The CSA uses dipole elements with interdigital fingers or overlapping arms to introduce the necessary interelement capacitance. The dipole elements are preferred for their UWB performance and achieving dual-linear polarization. For the TCPA, patch elements are employed for their better bandwidth performance in low-profile microstrip antennas. In this case, the interelement capacitance is obtained by the close proximity of the patches (and the reason the aperture is referred to as the TCPA). For the current design, single linear polarization is considered.

[9] 4. The dipole arms in the CSA are excited using two out-of-phase coaxial cables. This arrangement introduces the well-known common modes at the feed structure. Thus, a balun is necessary between the balanced dipole arms and the unbalanced coaxial cables. These difficulties are overcome in the TCPA arrangement using standard SMA coaxial probes to excite the patches. The probe feeds are actually brought toward patch edges to enable adjacent patch excitation to form the current sheet.

[10] 5. In finite realizations of the CSA, only elements toward the center are excited. The other elements toward the edges are terminated with resistors in an effort to suppress edge diffractions that deteriorate the radiation pattern and the impedance bandwidth of excited elements. However, radiation efficiency is typically reduced down to as low as 30% at the lowest operational frequency. For the TCPA, we also excite elements selectively. However, the passive elements are left open circuited for improved efficiency. In fact, the radiation efficiency reaches 97% while most of the loss is coming from the feeding network, reducing efficiency to 86%.

[11] In section 2, we begin by explaining the operational principle of the TCPA. We describe the unit cell and provide a step-by-step realization of the finite size TCPA. Section 3 presents the thin and compact microstrip feeding network for exciting the TCPA. In section 4, the TCPA is compared with a conventional patch antenna. Next, in section 5, measured results for a fabricated TCPA prototype are given. Conclusions are drawn in section 6.

2. Design of the Tightly Coupled Patch Array

2.1. Unit Cell Design

[12] FSSs have been typically constructed using closely spaced dipoles, while other element types are also possible [*Munk*, 2000]. In this regard, patch elements can be also viewed as a special case of dipoles (i.e., fat dipoles). For understanding, we can represent the FSSs using equivalent circuits, as depicted in Figure 1. Specifically, each dipole can be represented by an inductor of inductance L_d. Also, the coupling between dipoles can be represented by a series capacitance, C_d. Such an FSS resonates at $\omega_0 = 1/\sqrt{L_d C_d}$. At frequencies lower than this resonance, the FSS becomes capacitive. For HIS, AMC and EBG applications, such FSSs are placed on grounded dielectric slabs, as illustrated in Figure 1a (left). For the fundamental mode and the principle E and H planes, the grounded dielectric slab of thickness h can be considered as a short-ended transmission line. Thus, the impedance seen looking into the substrate, from the FSS plane, becomes $Z^+ = jZ_d \tan(\beta_d h)$. Obviously, Z^+ is inductive for thin substrates. Mushroom-type elements exhibit similar inductance with the insertion of vias. The resulting circuit model is shown in Figure 1a (right). As pointed out by *Costa et al.* [2009], although below the FSS resonance C_d term dominates over L_d, this series inductance should be still included in the model. In this case, the resonance frequency of the FSS on grounded dielectric slab becomes $\omega_0 = 1/\sqrt{(L_d + L_{gp})C_d}$. One important conclusion by *Costa et al.* [2009] was, in contrast to what would be expected from the easier parallel LC model that neglects the L_d term, increasing capacitance C_d does not decrease the HIS bandwidth of FSS on ground plane. On the contrary, tightly cou-

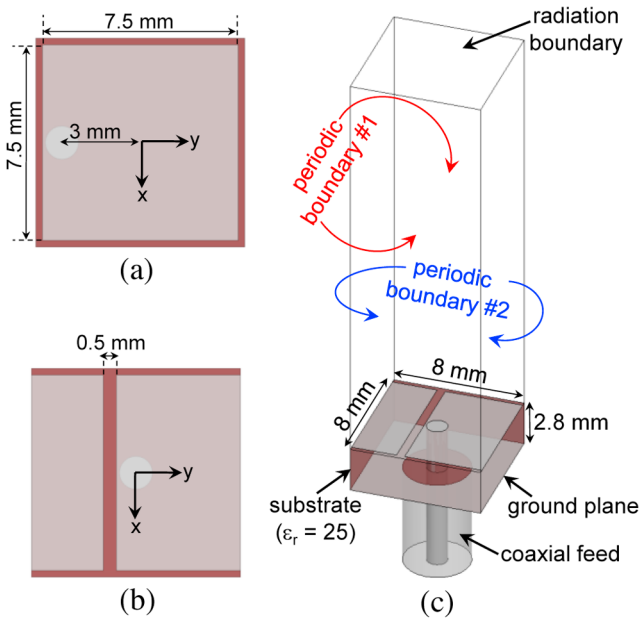

Figure 2. TCPA unit cell. (a) Top view. (b) Top view, shifted. (c) Three-dimensional view.

pled patches were shown to deliver much broader bandwidth than cross-type elements [*Costa et al.*, 2009].

[13] As noted earlier, past designs for low-profile antennas employed FSSs as substrates or ground planes underneath the main radiator (e.g., dipole, patch). This main radiator is usually capacitive below its natural resonance. The FSS on ground plane, which is inductive below its own resonance, was therefore used for canceling the capacitance of the main radiator [*Mosallaei and Sarabandi*, 2004]. As would be expected, this arrangement required FSSs with sufficient thickness to provide the necessary inductance. In several works [*Yang and Rahmat-Samii*, 2003b; *Mosallaei and Sarabandi*, 2004; *Sarabandi et al.*, 2006] it was observed that thickness of the FSS itself constitutes at least 2/3 of the overall antenna thickness. Clearly, this is an important hindrance to achieve very low profiles.

[14] Indeed, similar cancelation of inductance by capacitance is also employed in the CSA [*Munk*, 2003; *Munk et al.*, 2003], whose unit cell shown in Figure 1b (left). In essence, the CSA is an FSS on a ground plane, where the FSS itself is the radiator. Dipoles in (otherwise passive) FSS are excited periodically at their centers. Capacitances are introduced intentionally at the tips of neighboring dipole arms. Similar to the low-profile antennas on passive FSSs, this capacitance serves to cancel the inductance due to the ground plane, determining the lowest frequency of operation for the CSA. Consequently, the CSA can achieve a 4.5:1 UWB performance, while maintaining a low profile of $\lambda_0/10$ without using any dielectrics. In addition, the simple circuit models shown in Figures 1b (middle) and 1b (right) are substantially valid for calculating the input impedance, before grating lobes start appearing.

[15] In fact, the TCPA concept is mainly inspired by the impressive wideband and low-profile performance of the CSA. TCPA is intended to bring the benefits of such an array to the area of miniature microstrip antennas. Eventually, the goal is to achieve a small-size, very low profile (both physically and electrically), yet broadband and high-gain microstrip antenna. For this, we considered tightly coupled patch elements on a grounded high-contrast dielectric substrate (ε_r = 25, $\tan_\delta$ = 0.001; obtainable from Trans-Tech Inc. or TCI Ceramics), as illustrated in Figure 2. The HIS performance of such patches were already found to be very broadband in the passive FSS mode [*Costa et al.*, 2009]. The high-contrast dielectric substrate is preferred for miniaturizing the patch elements, therefore to be able to fit as many elements in a small finite volume. When tightly packed on this high-contrast dielectric, close proximity of patch elements also create enough capacitance (1.3 pF using the formulas given by *Mosallaei and Sarabandi* [2004]) to cancel the inductance due to the ground plane. This capacitance also acts as capacitive loading for additional miniaturization. For excitation, standard SMA probes feeds are used (probe radius: 25 mil, coaxial feed radius: 80 mil, filled with ε_r = 2 material). Each patch is excited periodically, at a point toward its left edge. Different from CSA, capacitive coupling and excitation sections of the unit cell are very close to each other. Since the probe feed is very close to the edge, its coaxial section exceeds the bounds of unit cell. To avoid this, the patch is shifted so that the feed stays in the middle of the unit cell, as shown in Figures 2b and 2c. This structure is simulated in Ansoft HFSS v12.1 by applying the periodic boundary conditions depicted in Figure 2c. This implies that each unit cell is excited periodically and uniformly.

[16] Active input impedance and returns loss obtained from the infinite TCPA are shown in Figure 3. Although the unit cell is very small and extremely low profile ($\lambda_0/20 \times \lambda_0/20 \times \lambda_0/57$ or $\lambda_g/4 \times \lambda_g/4 \times \lambda_g/11.4$ at 1.88 GHz), it has a broad impedance bandwidth (7.3% for $|S_{11}| < -10$ dB). This can be attributed to periodically exciting each unit cell, as in the case of CSA. Indeed, for such an array, the evanescent waves around one unit cell can only extend up to halfway into next unit cells [*Munk*, 2003]. If the same unit cell was to be used stand alone (in the absence of FSS array), these evanescent waves would extend into infinity [*Munk*, 2003]. Therefore, the TCPA has less evanescent waves, implying less stored energy (thus, lower Q) and broader bandwidth. In addition, it should be remarked that the TCPA element has very small extent (thus, periodicity). As in the case of tightly placed Gangbuster dipoles [*Munk*, 2000], or other unit cells in passive FSS mode [*Barbagallo et al.*, 2006], smaller periodicity also helps achieving broader bandwidth. This is again because the evanescent waves around each unit cell shrink to smaller physical space, hence decreasing stored energy and Q.

2.2. Design of the Finite Array

[17] For the finite array realization, we considered a small-size (4.8 cm × 4.8 cm × 2.8 mm) grounded dielectric substrate as shown in Figure 4a. Within this small area, the substrate can host 6 × 6 = 36 TCPA unit cells. The leftmost column of the array was left unexcited due to the proximity of the coax feeds, to avoid edge disruptions. Thus, the remaining 30 ports are excited uniformly, as shown in Figure 4b. A close inspection reveals that, each feed also capacitively excites the neighboring patch to its left, as illustrated in Figure 4c. In this manner, two adjacent patches can be considered as the arms of a fat dipole, fed at the center. Therefore, a current sheet is

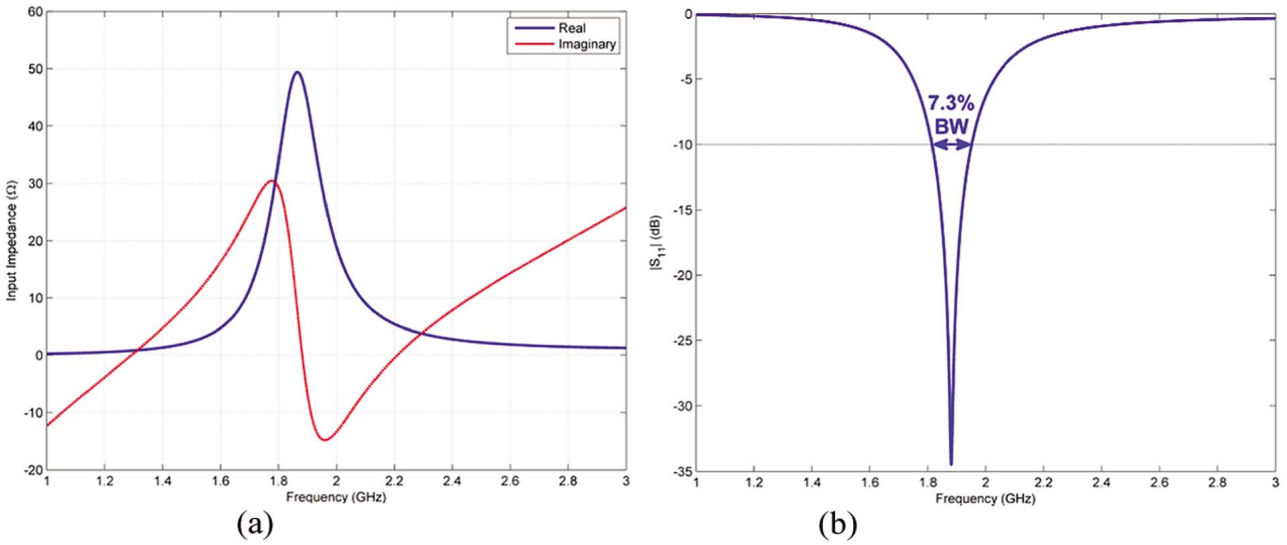

Figure 3. TCPA unit cell performance. (a) Input impedance. (b) Return loss.

formed on the TCPA aperture, flowing through the overlapping arms of these dipoles.

[18] Next, active return losses of the 30 uniformly excited elements are computed, as depicted in Figure 5a. Due to the symmetry in the array, only results for upper half of the array are shown (which is also implied for the rest of the results in this manuscript). From Figure 5a, it is observed that all elements (except those on the two rightmost columns) resonate around 2 GHz, which is close to 1.88 GHz (expected from infinite array). The elements on the two rightmost columns resonate at slightly higher frequencies. This is a classical manifestation of truncating the substrate in finite arrays. Such finite edges cause wave bounces and diffractions from the dielectric/air boundaries. Since the elements on these two columns were found to be "problematic," we next consider the case where these elements are not excited. Although these elements are not excited, the coaxial probes still remain in place, thus these ports are terminated with 50Ω impedances. The new active return losses for the remaining 18 excited elements are shown in Figure 5b. Figure 5c shows these return losses plotted on top of each other. It can be observed that for this case, all 18 excited elements resonate at 2 GHz.

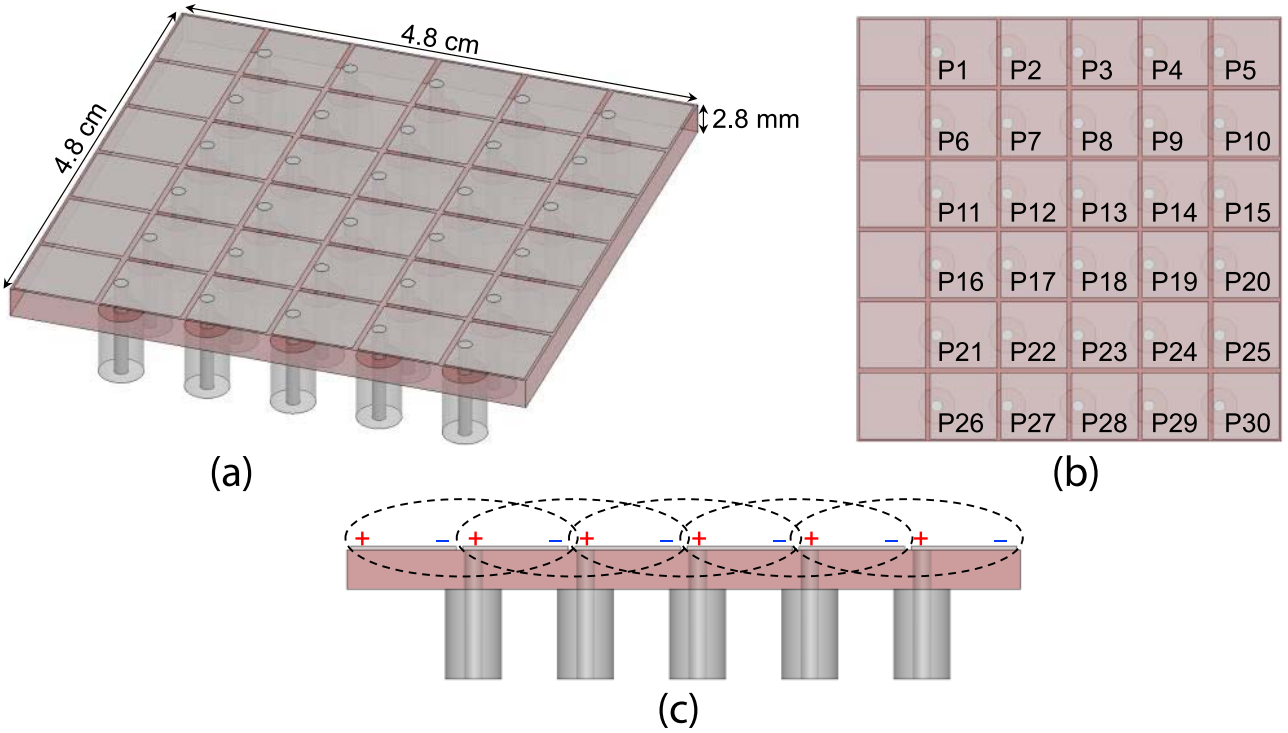

Figure 4. Finite 6 × 6 TCPA array with 30 excited elements. (a) Three-dimensional view. (b) Top view. (c) Side view.

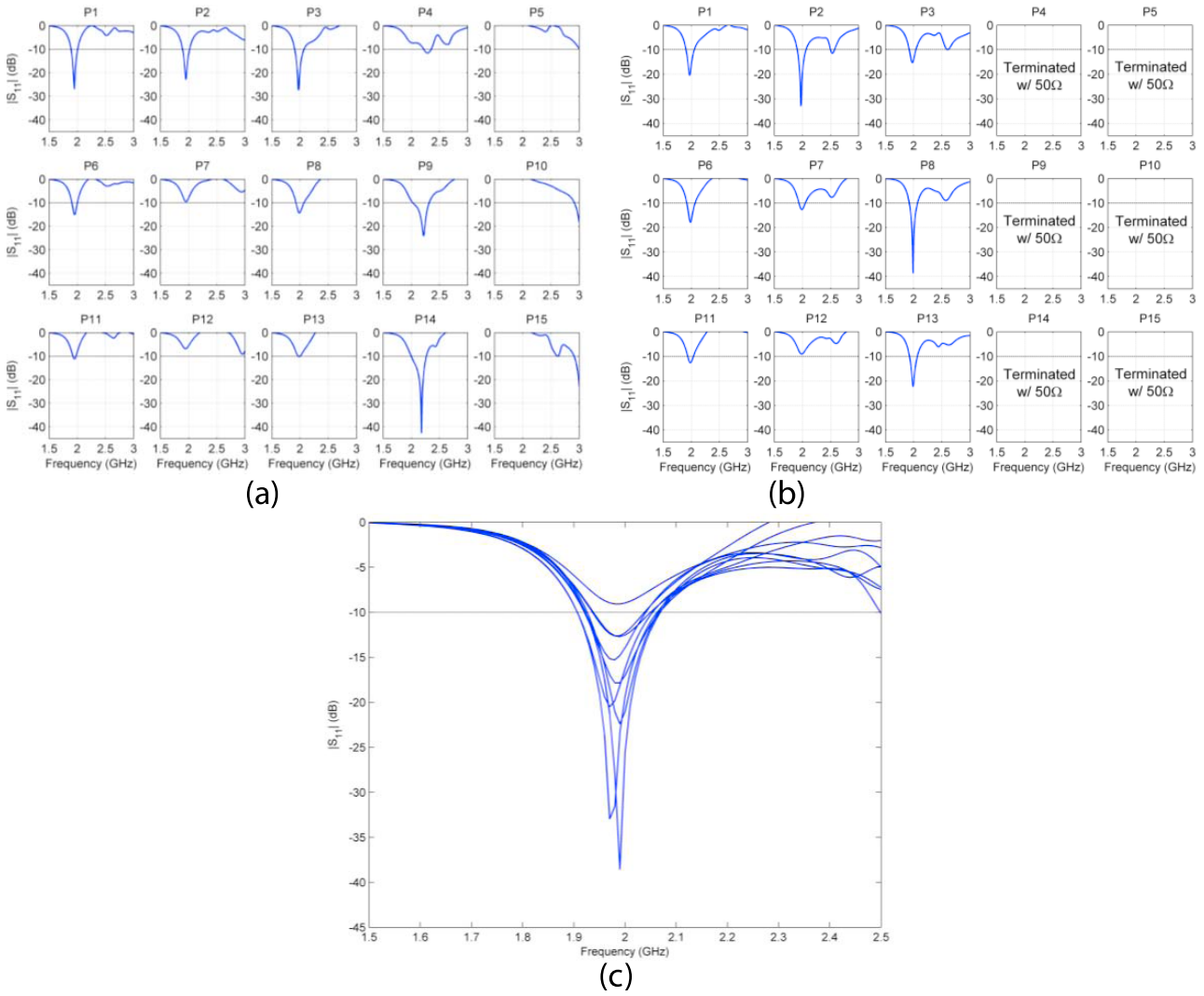

Figure 5. Active return losses of (a) 30 excited elements; (b) 18 excited elements, 12 terminated with 50Ω; and (c) 18 excited elements, 12 terminated with 50Ω, plotted together.

A comparison of return losses in Figures 5a and 5b together revealed that the response for these 18 elements change only slightly.

[19] Although Figure 5c shows great promise, it should be remarked that the probe feeds with 50Ω termination impedances would dissipate the power delivered to them. Evidently, this decreases the antenna efficiency significantly. Moreover, such resistive antenna loads are not desired for high-power applications. In addition, although unexcited, probe feeds need to be connected to these patches, which is uncalled for. In the next step, we considered leaving the unexcited ports as open circuited (parasitic patches), rather than terminating with 50Ω loads. The new geometry and numbering of ports are shown in Figure 6. Active return losses corresponding to this case are shown in Figure 7a for each individual port; and in Figure 7b for all ports together. It is observed that only ports 6, 9 (and their symmetric ones 12, 15) resonate at a slightly higher frequency. As done previously, we next terminate two of these ports (9 and 12) with 50Ω loads. The resulting active return losses for the remaining 16 excited ports are shown in Figures 7c and 7d. Again, all remaining excited ports now resonate at the same frequency, i.e., 2 GHz.

[20] As the next step, the process explained above is repeated by considering only 16 excited elements, while the rest are left open. The new TCPA geometry is shown in Figure 8a. Similar to previous observations, active return losses for these ports (shown in Figures 8b and 8c) indicate that only 2 of the excited ports (now 6 and 13, were 6 and 15 in previous) resonate at a slightly higher frequency. These two ports can be also considered to be terminated or left open, and the process for choosing which elements to excite can be carried out in this manner until acceptable performance is achieved. However, we opted to discontinue such design iterations at this point. As the main reason, it can be remarked that the total number of excitations are now 16, which happens to be a power of 2. This would make the feeding network design (to be discussed in section 3) much easier.

[21] One critical observation from Figures 5, 7, and 8 was the poor impedance matching for some of the ports. Although most ports resonated at around 2 GHz, investigation of the return losses revealed that their input impedances were not

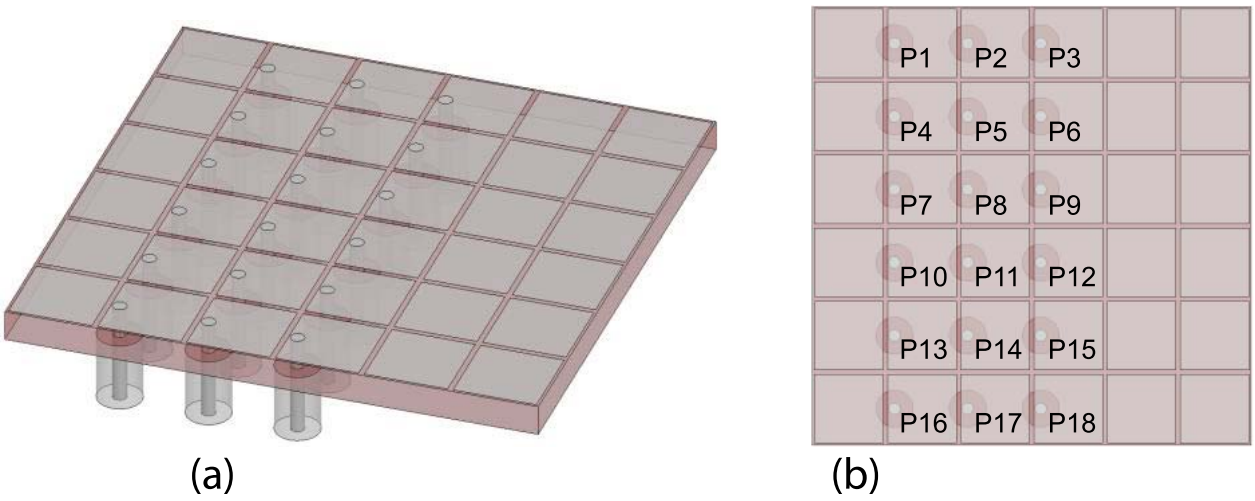

Figure 6. Finite 6 × 6 TCPA array with 18 excited elements. (a) Three-dimensional view. (b) Top view.

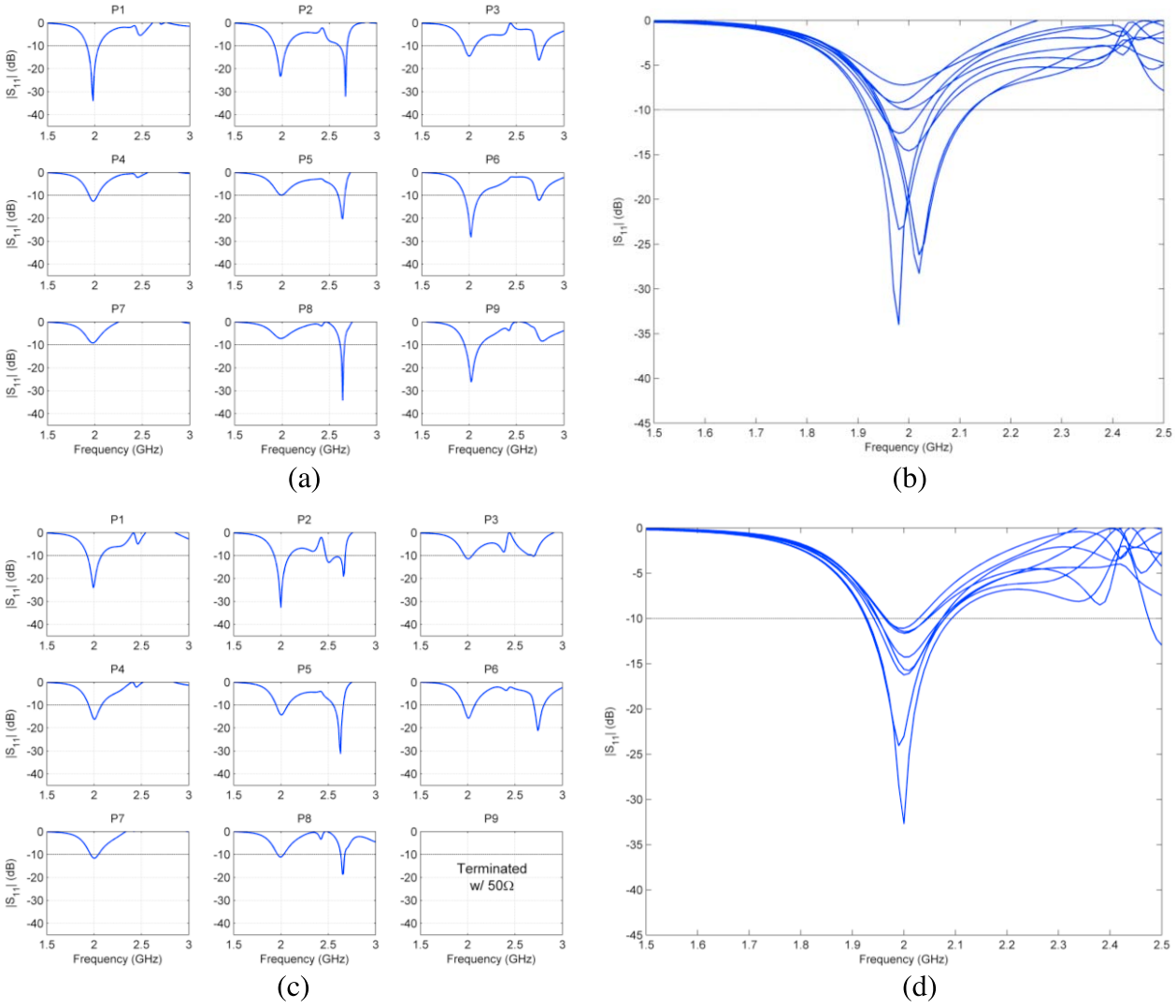

Figure 7. Active return losses of (a) 18 excited elements; (b) 18 excited elements, plotted together; (c) 16 excited elements, ports 9 and 12 terminated with 50Ω; and (d) 16 excited elements, ports 9 and 12 terminated with 50Ω, plotted together.

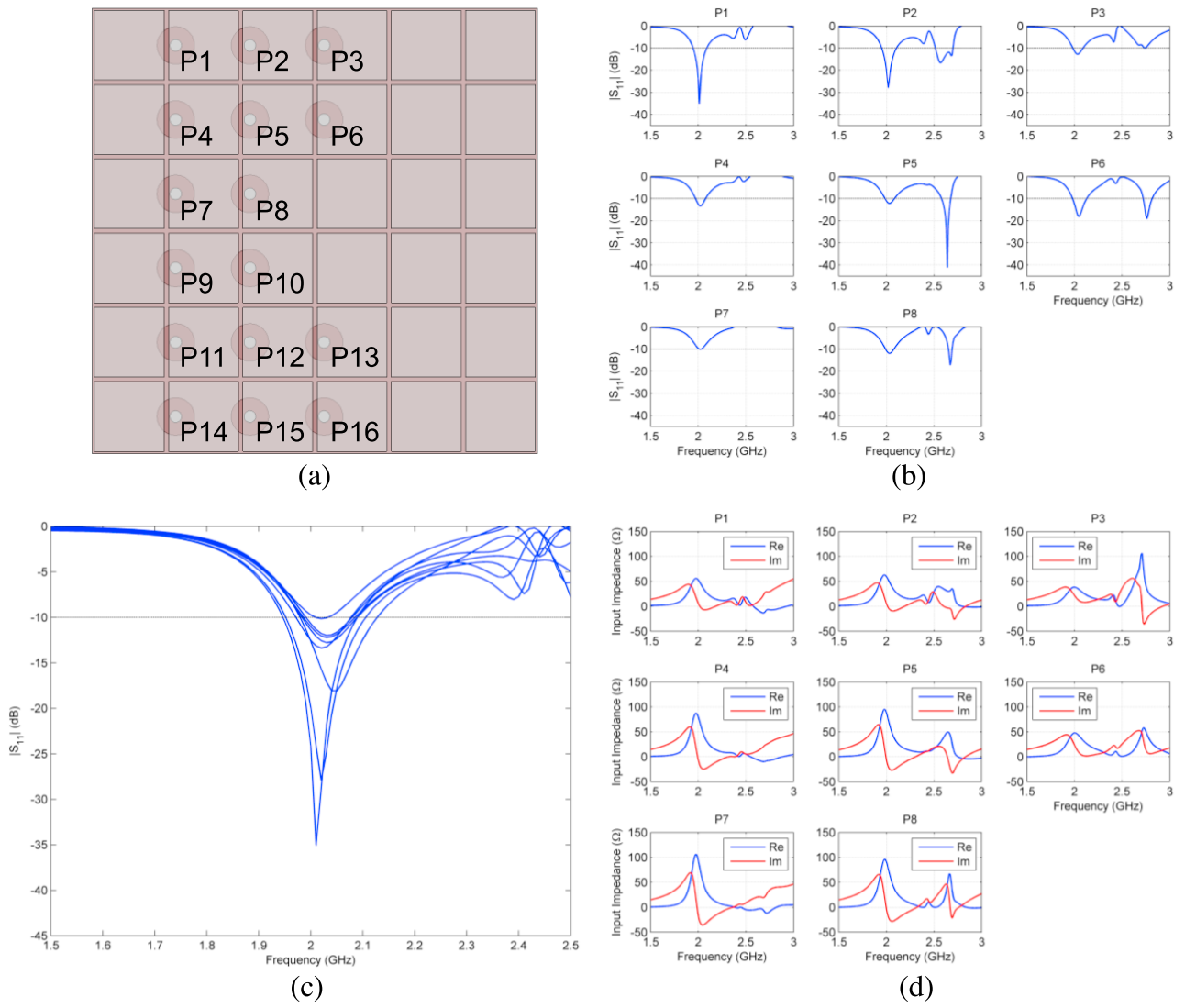

Figure 8. (a) Finite 6 × 6 TCPA array with 16 excited elements, top view. (b) Active return losses of 16 excited elements. (c) Active return losses of 16 excited elements, plotted together. (d) Active input impedances of 16 excited elements.

exactly 50Ω. In Figure 8d, real and imaginary parts of the input impedance for each excited port are also shown, which corresponds to the geometry in Figure 8a. Indeed, real parts of the input impedance for ports 4, 5, 7, 8, 9, 10, 11 and 12 were much higher than expected (in the orders of 90Ω–110Ω). Ports 3 and 16, on the other hand, were observed to be close to 40Ω. As explained earlier, such disruptions stemmed from truncation of the finite array. Fortunately, real part of the input impedance for each excited port can be decreased or increased simply by moving the probe feed closer to or away from center of the patch, respectively. To avoid creating other modes and cross polarization, the feeds are only moved along the *y* axis. Indeed, after a few iterative steps of concurrent fine tuning, the feed positions shown in Figure 9a were found optimal for best impedance matching. Figure 9b shows the new input impedances for excited elements. It can be observed that real parts of input impedances are close to 50Ω for all patches, at their resonant frequencies. Corresponding return losses are given in Figures 9c and 9d, which indicate that resonance frequencies of the excited patches move to slightly higher frequencies. While each patch has about 7.2% impedance bandwidth, their resonance frequencies are not exactly overlapping. These patches continuously cover an 8.8% band, centered around 2.07 GHz. The overlapping band, where they all have $|S_{11}| < -10$ dB, is about 5.8%. Thus, if the patches are to be excited using the same signal source, (possibly making use of a feeding network), the overall impedance bandwidth would be close to 5.8%. Clearly, the resonance frequencies of all patches can be optimized to overlap exactly, by adjusting the size of each individual patch. In this case, the overall impedance bandwidth can be increased to 7.2%. However, this option is left as future work. In summary, the geometry and results in Figure 9 constitute the final version of the finite size TCPA designed

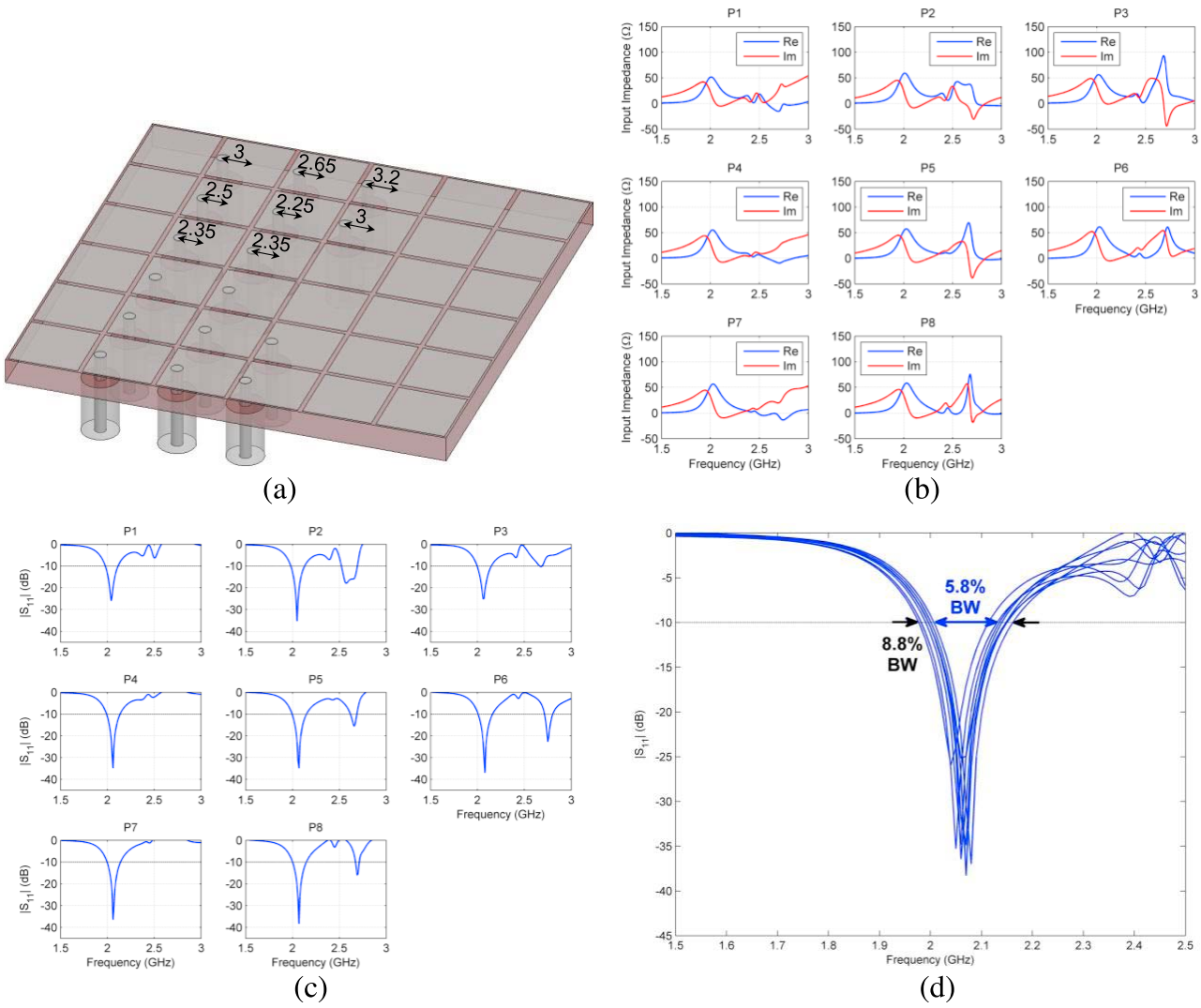

Figure 9. Finite 6 × 6 TCPA array with 16 excited elements having optimized feed locations (distances in mm), 3-D view. (b) Active input impedances of 16 excited elements. (c) Active return losses of 16 excited elements. (d) Active return losses of 16 excited elements, plotted together.

here. We remark that, at 2.07 GHz, this TCPA has the electrical size of $\lambda_0/3 \times \lambda_0/3 \times \lambda_0/52$. Yet, this extremely thin TCPA achieves a realized gain of 5 dB (97% efficiency).

3. Design of the Feeding Network

[22] The TCPA designed in section 2 utilizes standard 50Ω SMA probes. Therefore, it is quite possible to feed it using an external feeding network. Since the TCPA has 16 ports, there are various ways of forming such a feeding network. The easiest option would be to use a 16-way equal power divider. Alternatively, one can use 8-way, 4-way or 2-way power dividers and combine them to form a multistage power divider. However, such external power dividers are usually bulky, expensive and more importantly, they can have high insertion losses. To avoid these, in this section we design a compact microstrip feeding network, which is also very thin. This network employs four stages of 2-way equal power dividers (i.e., Wilkinson power divider).

[23] A major difficulty associated with the feeding network is the limited space under the antenna. Due to small size of patch elements, miniaturized dividers are called for. A design guideline for realizing such miniature dividers was given by *Kangasvieri et al.* [2006], where the $\lambda_g/4$ sections of the Wilkinson divider were miniaturized via meandering. This design is adopted for 2.07 GHz center frequency and its corresponding layout is shown in Figure 10a. As the substrate, a 25 mil thick Rogers RO3010 (ε_r = 10.2, $\tan_\delta$ = 0.0023) is used. Correspondingly, widths of the microstrip lines with 50Ω and 70.7Ω characteristic impedances are 22 mil and 9 mil, respectively. Of course, using a higher-permittivity dielectric substrate would help miniaturization. However, in that case the microstrip lines need to be much narrower. Clearly this is not desirable, since such very narrow microstrip lines would create difficulties in fabrication. The narrowest microstrip line employed here is 9 mil, which can be fabricated using standard milling or screen printing techniques.

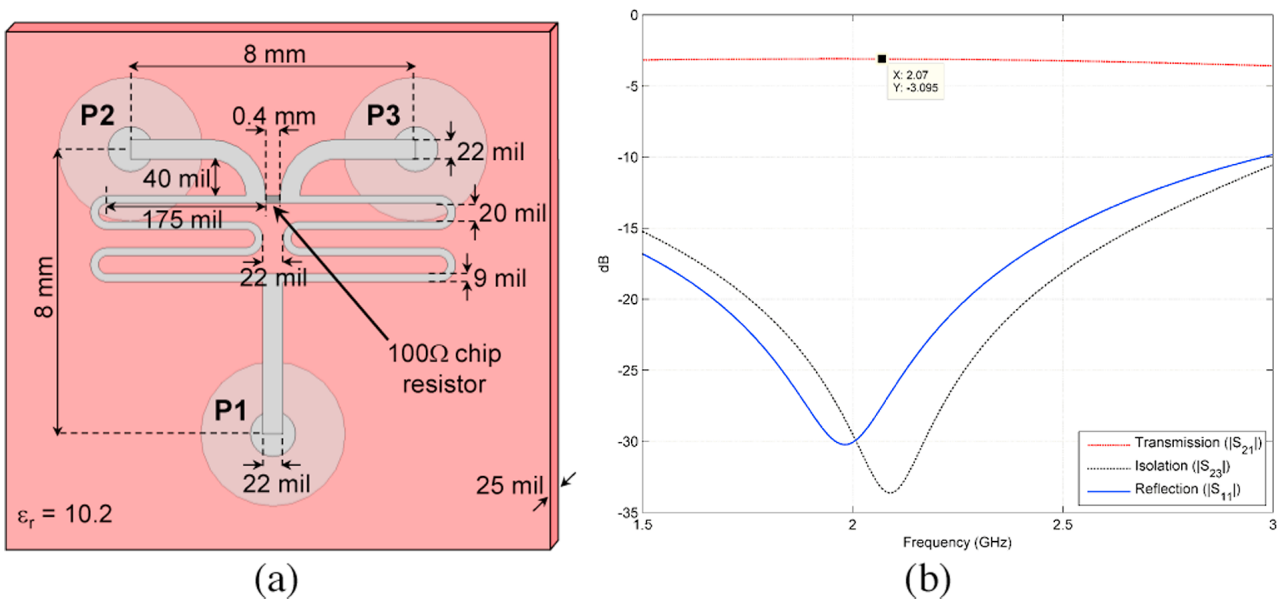

Figure 10. Single stage Wilkinson power divider. (a) Geometry. (b) Frequency response.

[24] Since the substrate is very thin, and microstrip lines are narrow, conductivity losses become important. To take into their effects, metallizations on both sides of the substrate are modeled as 3-D copper plates with 35 μm thickness (1 oz cladding). A small-size (0.4 mm × 0.2 mm) chip resistor from Panasonic ERJXGN series is also employed for improving isolation. The transmission, isolation and reflection performance of this divider is shown in Figure 10b. It is observed that the isolation and reflection levels are good across the whole band. Insertion loss is around 3.1 dB, which is only 0.1 dB higher than the theoretical value (3 dB). Thus, after four stages of such dividers, a total of 0.4 dB insertion loss (in addition to 12 dB theoretical) can be expected.

[25] The desired 16-way power divider network is formed by cascading 4 stages of Wilkinson power dividers designed above. Input/output ports of the network are included as standard SMA probes. One necessary requirement for the TCPA is having uniform excitations. Therefore, microstrip line sections from input port to all output ports are adjusted to be the same length. As in Wilkinson divider case, metallizations are modeled as 35 μm thick copper plates. Layout of the final feeding network is shown in Figures 11a and 11b. Reflection seen at the input port is given in Figure 11c, which exhibits the required broadband performance. In addition, transmissions from the input port to each of the output ports are examined. It is found that the insertion loss is 0.5 dB ± 0.7 dB (in addition to 12 dB theoretical). The phase variations are ±6°.

4. Integrated Antenna Performance and Comparisons to Other Antennas

[26] In this section, integrated performance of the TCPA (i.e., array + feed) is evaluated by comparison to a conventional patch antenna having same overall dimensions. First, the array part of the TCPA designed in section 2 is combined with the feeding network designed in section 3. This is done by removing the SMA probes underneath the array and above the feeding network ground planes and directly combining the two. Thus, the array and the feed network utilize the same ground plane, while the circular holes with 80 mil radius (which were opened to host coaxial feeds) remain intact. Then, the microstrip lines of the feeding network are connected to the patches using vias (with 25 mil radius, same as probe feeds). The layout of the TCPA in its final form is shown in Figure 12a. In the HFSS model, all metallic parts are copper, including patches, vias, ground plane and the microstrip lines. Therefore, all conductivity and dielectric losses are accounted for. Total thickness of the TCPA including its feeding network becomes 135 mil. The computed impedance bandwidth of this TCPA prototype is 5.6% at 2.07 GHz. This is very close to the 5.8% bandwidth previously expected from Figure 8d. However, due to insertion losses in its feeding network (0.6 dB), its realized gain drops to 4.4 dB, reducing its efficiency from 97% to 86%. It is noted that the small amplitude and phase misbalances in the feed did not affect the radiation pattern appreciably. At 2.07 GHz, the overall dimensions of the TCPA are $\lambda_0/3 \times \lambda_0/3 \times \lambda_0/42$, which is an extremely thin antenna.

[27] For comparison purposes, several conventional patch antennas were considered. The aim was to find an antenna having the same overall dimensions with the TCPA, while providing the broadest impedance bandwidth. Since the TCPA utilizes almost all of its substrate, a seemingly logical choice would be to use a large patch, extending to the limits of the substrate. However, to be able to resonate at the same frequency with the TCPA, such a patch needs to be placed on a low-contrast dielectric substrate. For fixed physical thickness, this would make the substrate electrically thinner (with respect to guided wavelength). Thus, such large patch antennas on low-contrast substrates have very narrow bandwidths (about 0.5%). Another choice was connecting the excited patches of the TCPA, forming a U-shaped patch. In addition, using parasitic patches around this U-shaped patch (as was in the case of TCPA) was also considered. Neither of these approaches could exceed 1% bandwidth. The best

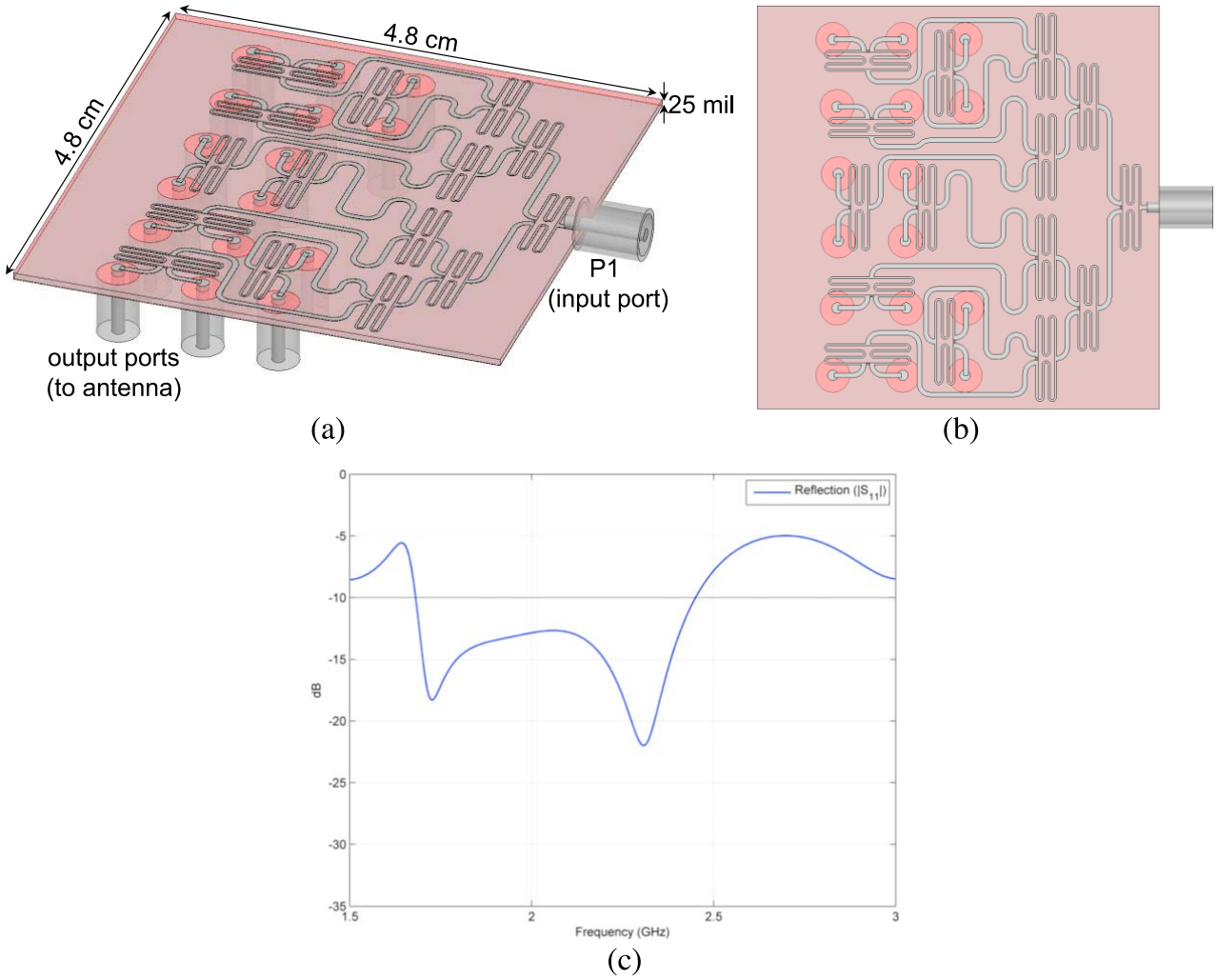

Figure 11. Multiple-stage, 16-way, equal power division and feeding network. (a) Geometry, reversed 3-D view. (b) Geometry, bottom view. (c) Frequency response.

impedance bandwidth was obtained, however, using a rectangular patch on high-contrast dielectric substrate ($\varepsilon_r = 25$). Layout of this antenna is shown in Figure 12b. This rectangular patch could create two resonances and was matched to 50Ω in between. However, since the substrate is thin, the resonances are very narrowband. This reduces the impedance bandwidth significantly. The broadest impedance bandwidth obtained after optimization was 2.5% at 2.07 GHz. Figure 13a compares the input impedance of the TCPA and this conventional patch. Realized gain of the patch antenna was

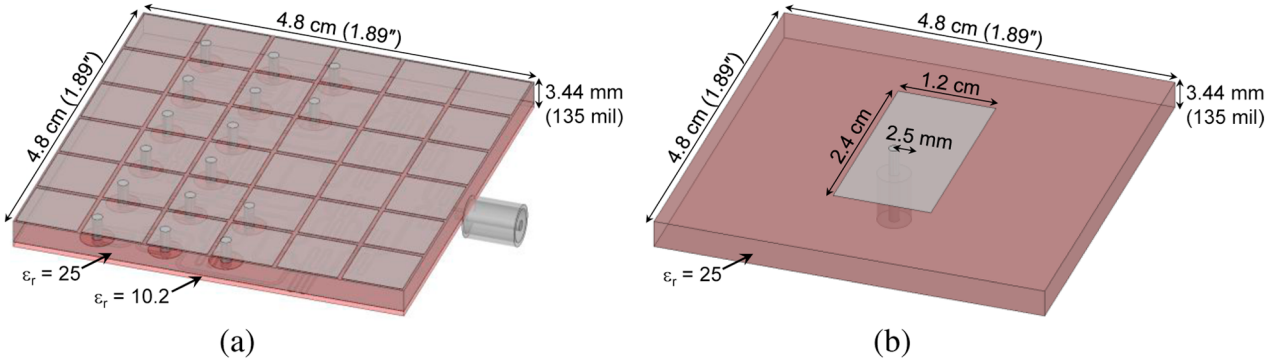

Figure 12. Layouts of (a) TCPA and (b) conventional patch antenna.

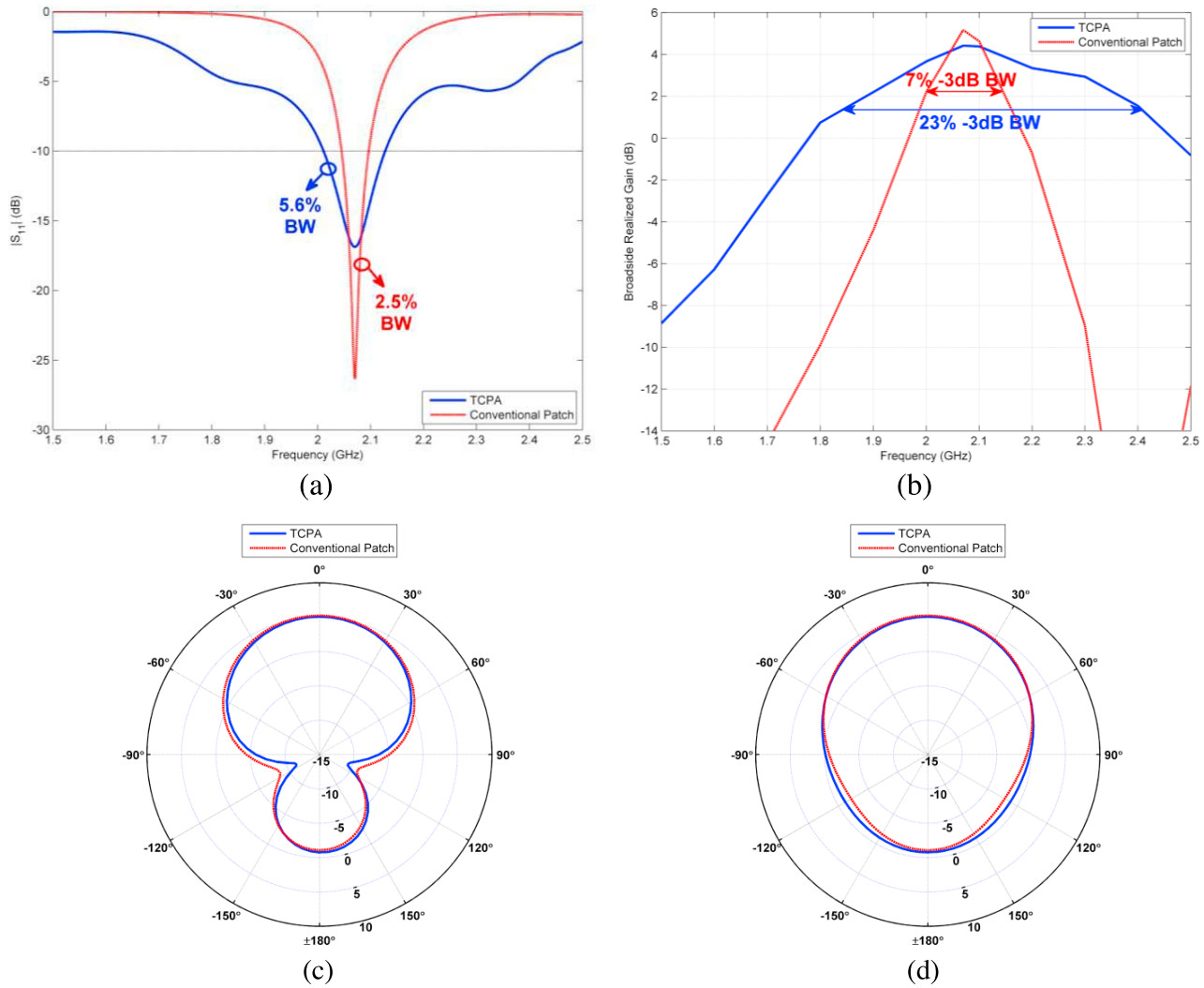

Figure 13. Performance comparison of TCPA versus conventional patch antenna. (a) Return losses. (b) Realized gains in broadside direction. (c) Radiation patterns in E plane. (d) Radiation patterns in H plane.

as high as 5.16 dB, however, decreased very sharply with frequency. The realized gains in broadside direction are compared in Figure 13b, where it is revealed that TCPA can also maintain a very broad gain bandwidth. This is mainly because TCPA creates a current sheet on the antenna aperture which does not fluctuate abruptly with frequency. The radiation patterns of the TCPA and conventional patch were found to be very similar, as shown in Figures 13c

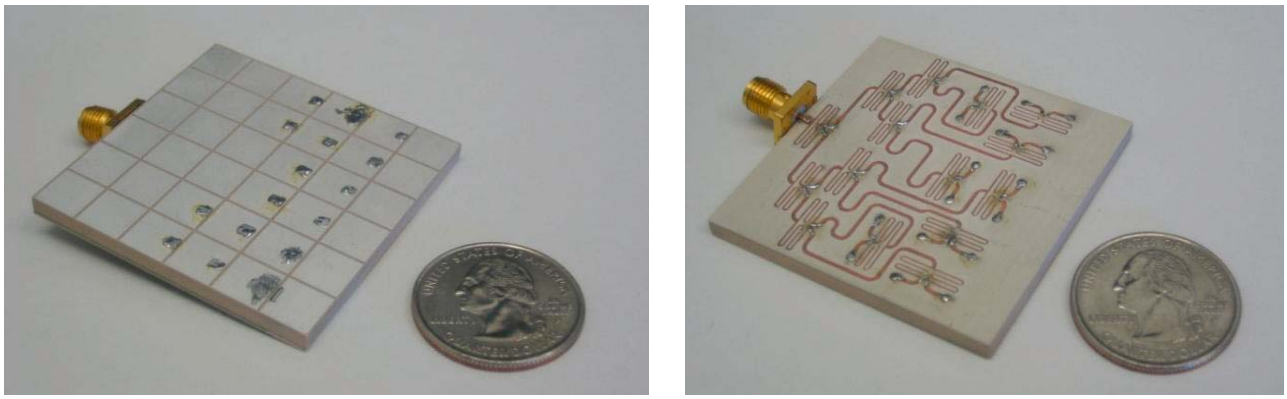

Figure 14. Fabricated TCPA prototype. (a) Front view. (b) Back view.

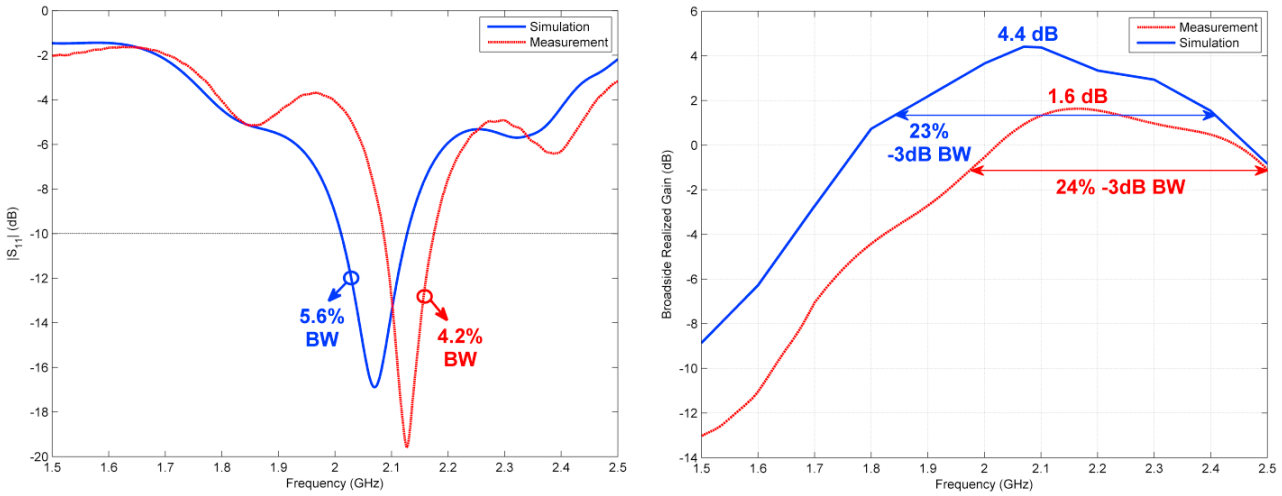

Figure 15. Measured return loss and realized gain of the TCPA prototype in Figure 14. (a) Return loss. (b) Realized gain at broadside.

and 13d. This similarity also applies to their cross polarization levels.

5. Experimental Verification

[28] A TCPA prototype was built and tested at The Ohio State University ElectroScience Laboratory and is shown in Figure 14. The patch array was screen printed using a high-conductivity silver ink. The feeding network was fabricated using a milling machine with small chip resistors soldered (as needed) to improve isolation. The measured return loss gave 4.2% bandwidth at 2.13 GHz (with a small frequency shift and little less than the 5.6% computed) and is shown in Figure 15a. This difference is likely due to a possible air gap formed between the ground plane and array substrate and the sensitivity of probe feed positions. The latter could have caused a slight nonoverlap of the individual patch resonances.

[29] The broadside realized gain of the fabricated TCPA prototype was measured in the anechoic chamber. From Figure 15b, we observe a peak realized gain of 1.6 dB (50% efficiency) at 2.15 GHz. This is 3 dB smaller than the computed gain with the difference attributed to conductivity losses in the silver ink and soldering. This prototype had very thin silver cladding (16 μm) with poor conductivity to augment conductivity losses. We remark that such conductivity losses would be also present for the conventional patch, if fabricated.

6. Conclusions

[30] A small-size and low-profile antenna array was designed using tightly coupled patch elements. Due to its small periodicity and tight placement, these patches serve as a broadband frequency selective surface. Rather than using a secondary radiating element (typically placed above), this FSS itself was used as the main radiator. While the former method is employed very commonly in the open literature for realizing low-profile antennas, the latter enabled achieving much reduced profile with more enhanced impedance and realized gain bandwidths as compared to conventional patch antennas. This much broadband performance was mainly due to small periodicity and periodic excitation of the FSS, which helped reducing the stored electromagnetic energy underneath the antenna. In essence, this created an effective current sheet on the antenna aperture that does not fluctuate abruptly with frequency and utilizes the whole substrate as efficiently as possible. Finally, the TCPA can be also considered as a segmented (or fragmented) patch with multiple selective feeds. For conventional patches, radiation occurs from the radiating slots (magnetic line currents). For the patch array, the magnetic currents are between adjacent patches to represent the slots formed among the patches. In this context, the TCPA demonstrates the advantages of using such segmented patches instead of a single and connected patch with a single feed.

[31] **Acknowledgments.** This work was supported by the U.S. Army Research Laboratory, Adelphi, Maryland (through Applied EM Inc. under contract W911QX-10-C-0064). The authors would like to thank Lanlin Zhang for screen printing the patch array and Ugur Olgun for his help and guidance during milling of the feeding network.

References

Barbagallo, S., A. Monorchio, and G. Manara (2006), Small periodicity FSS screens with enhanced bandwidth performance, *Electron. Lett.*, *42*(7), 382–384, doi:10.1049/el:20060329.

Bell, J., and M. Iskander (2004), A low-profile archimedean spiral antenna using an EBG ground plane, *IEEE Antennas Wireless Propag. Lett.*, *3*(1), 223–226, doi:10.1109/LAWP.2004.835753.

Bell, J. M., M. F. Iskander, and J. J. Lee (2007), Ultrawideband hybrid EBG/ferrite ground plane for low-profile array antennas, *IEEE Trans. Antennas Propag.*, *55*(1), 4–12, doi:10.1109/TAP.2006.888455.

Costa, F., S. Genovesi, and A. Monorchio (2009), On the bandwidth of high-impedance frequency selective surfaces, *IEEE Antennas Wireless Propag. Lett.*, *8*, 1341–1344, doi:10.1109/LAWP.2009.2038346.

Erdemli, Y., K. Sertel, R. Gilbert, D. Wright, and J. Volakis (2002), Frequency-selective surfaces to enhance performance of broadband reconfigurable arrays, *IEEE Trans. Antennas Propag.*, *50*(12), 1716–1724, doi:10.1109/TAP.2002.807377.

Feresidis, A., G. Goussetis, S. Wang, and J. Vardaxoglou (2005), Artificial magnetic conductor surfaces and their application to low-profile

high-gain planar antennas, *IEEE Trans. Antennas Propag.*, *53*(1), 209–215, doi:10.1109/TAP.2004.840528.

Goussetis, G., A. Feresidis, and J. Vardaxoglou (2006), Tailoring the AMC and EBG characteristics of periodic metallic arrays printed on grounded dielectric substrate, *IEEE Trans. Antennas Propag.*, *54*(1), 82–89, doi:10.1109/TAP.2005.861575.

Kangasvieri, T., I. Hautajärvi, H. Jantunen, and J. Vähäkangas (2006), Miniaturized low-loss wilkinson power divider for RF front-end module applications, *Microwave Opt. Technol. Lett.*, *48*, 660–663, doi:10.1002/mop.21436.

Mosallaei, H., and K. Sarabandi (2004), Antenna miniaturization and bandwidth enhancement using a reactive impedance substrate, *IEEE Trans. Antennas Propag.*, *52*(9), 2403–2414, doi:10.1109/TAP.2004.834135.

Munk, B. A. (2000), *Frequency Selective Surfaces—Theory and Design*, John Wiley, New York.

Munk, B. A. (2003), *Finite Antenna Arrays and FSS*, John Wiley, New York.

Munk, B., et al. (2003), A low-profile broadband phased array antenna, in *Antennas and Propagation Society International Symposium, 2003*, vol. 2, pp. 448–451, Inst. of Electr. and Electron. Eng., New York, doi:10.1109/APS.2003.1219272.

Sarabandi, K., A. Buerkle, and H. Mosallaei (2006), Compact wideband UHF patch antenna on a reactive impedance substrate, *IEEE Antennas Wireless Propag. Lett.*, *5*(1), 503–506, doi:10.1109/LAWP.2006.886302.

Sievenpiper, D., L. Zhang, R. Broas, N. Alexopolous, and E. Yablonovitch (1999), High-impedance electromagnetic surfaces with a forbidden frequency band, *IEEE Trans. Microwave Theory Tech.*, *47*(11), 2059–2074, doi:10.1109/22.798001.

Vardaxoglou, J. C. (1997), *Frequency Selective Surfaces: Analysis and Design*, John Wiley, New York.

Yang, F., and Y. Rahmat-Samii (2003a), Microstrip antennas integrated with electromagnetic band-gap (EBG) structures: A low mutual coupling design for array applications, *IEEE Trans. Antennas Propag.*, *51*(10), 2936–2946, doi:10.1109/TAP.2003.817983.

Yang, F., and Y. Rahmat-Samii (2003b), Reflection phase characterizations of the EBG ground plane for low profile wire antenna applications, *IEEE Trans. Antennas Propag.*, *51*(10), 2691–2703, doi:10.1109/TAP.2003.817559.

E. Irci, K. Sertel, and J. L. Volakis, ElectroScience Laboratory, Department of Electrical and Computer Engineering, Ohio State University, 1330 Kinnear Rd., Columbus, OH 43212, USA. (irci.1@osu.edu)